

Robust Regression with Highly Corrupted Data via Physics Informed Neural Networks

Wei Peng^a, Wen Yao^{a,*}, Weien Zhou^a, Xiaoya Zhang^a, Weijie Yao^b

^aDefense Innovation Institute, Chinese Academy of Military Science, Beijing, 100071, China

^bCollege of Aerospace Science and Engineering, National University of Defense Technology, Changsha, China

Abstract

Physics-informed neural networks (PINNs) have been proposed to solve two main classes of problems: data-driven solutions and data-driven discovery of partial differential equations. This task becomes prohibitive when such data is highly corrupted due to the possible sensor mechanism failing. We propose the Least Absolute Deviation based PINN (LAD-PINN) to reconstruct the solution and recover unknown parameters in PDEs – even if spurious data or outliers corrupt a large percentage of the observations. To further improve the accuracy of recovering hidden physics, the two-stage Median Absolute Deviation based PINN (MAD-PINN) is proposed, where LAD-PINN is employed as an outlier detector followed by MAD screening out the highly corrupted data. Then the vanilla PINN or its variants can be subsequently applied to exploit the remaining normal data. Through several examples, including Poisson’s equation, wave equation, and steady or unsteady Navier-Stokes equations, we illustrate the generalizability, accuracy and efficiency of the proposed algorithms for recovering governing equations from noisy and highly corrupted measurement data.

Keywords: Meshless method, Robust regression, PDEs

1. Introduction

Recently, with the explosive growth of available data and computational resources, deep learning has attracted tremendous attentions in recent years in the field of computational mechanics due to its powerful capability in nonlinear modeling of complex spatiotemporal systems. One seminal work in this direction is the Physics-Informed Neural Network (PINN)[1] approach introduced in a series of papers, which parameterizes a PDE’s solution as a neural network.

The general framework of PINN demonstrated its capacity in modeling complex physical systems such as solving/identifying PDEs. PINN can also exploit the available measurement data, making it possible to discover the systems whose physics are not fully understood. In particular, contributions of using PINN to model various physics have been made recently. For example, the Navier-Stokes equations are incorporated with data to reveal hidden fluid dynamics [2, 3] via PINN. Jin et al. [4] employed PINN to model incompressible flow from laminar to

*Corresponding Author

Email addresses: weipeng0098@126.com (Wei Peng), wendy0782@126.com (Wen Yao), weienzhou@nudt.edu.cn (Weien Zhou)

Preprint submitted to Null

October 20, 2022

turbulent. Sun et al. [5] proposed PINN-based surrogates of fluids in an unsupervised manner. Haghghat et al. [6] used PINN for inversion and surrogate modeling in the field of solid mechanics. Cai et al. [7] investigated solutions to various prototype heat transfer problems. He et al. [8] studied the problem of direct and inverse heat conduction in materials. Lu et al. [9] used PINN in reverse design to solve the holographic problem in optics and the fluid problem of Stokes flow.

With L_2 loss being one of the most popularly used metric, the vanilla PINN calculates the squared L_2 norm of the PDE and initial/boundary condition residuals on the domains, respectively. By defining differentiable loss functionals that measure how well the model fits PDEs and boundary conditions, the PINN parameters can be optimized using gradient-based approaches. A series of extensions to the vanilla PINN has been proposed to improve the accuracy and efficiency of handling increasingly challenging problems. Such extensions include, but are not limited to, tuning of loss weights [10, 11, 12, 13], novel network architectures and activation functions [14, 15, 16, 17], domain decomposition methods [18, 19], and collocation generation algorithms [20, 21, 22, 23, 24].

In the view of regression analysis, vanilla PINN is a nonlinear extension to the Ordinary Least Square (OLS) method, which we also refer to as OLS-PINN. Although previous PINN methods have demonstrated promising results by combining nonlinear regression with physics-informed regularizers, it is still absent for studies and improvements of PINN on highly corrupted data. Unfortunately, like OLS in linear analysis, the data-driven part of vanilla PINN (OLS-PINN) also suffers from highly corrupted data and thus fails to reconstruct solutions or parameters correctly. Fortunately, in the field of robust linear analysis, the M-estimator method has been used to relieve the data corruption issue, inspired by which, we attempt to develop robust PINNs for highly corrupted observation data.

This paper focuses on applying PINN to inverse problems, especially in the cases of incomplete boundary conditions, where solutions or parameters of the PDE equation are required to be recovered from observations that may be highly corrupted. The contributions of this paper are as follows.

1. We propose the LAD-PINN model inspired by the traditional LAD (Least Absolute Derivation) approach, where the L_1 loss replaces the squared L_2 data loss in OLS-PINN. A systematic numerical comparison is performed on various cases of multiple data corruption types, including anomalous and spurious data. It is found that the LAD-PINN is much more robust in recovering solutions from highly corrupted observations compared to the vanilla counterpart.
2. Motivated by the multi-stage robust linear regression methods such as REWLS or RANSAC[25], we further propose a two-stage algorithmic framework using LAD-PINN as the outlier detector. In particular, we propose a data cleaning process based on mean absolute derivation (MAD) and then solve PDEs or reconstruct solutions on the cleaned data.
3. PINN is a simple and practical approach to fuse data with physics, the popularity of which may come from its simplicity. Therefore, in this paper, the introduction of additional hyperparameters is minimized in the algorithm design, and even for the two-stage algorithm, only one interpretable hyperparameter is introduced. The number of remaining parameters is kept consistent with vanilla PINN. The work in this paper can be easily reproduced and applied to various fields, and the code for reproducing the experiments is available on <https://www.github.com/weipeng0098/robust-PINN>.

Related work. One class of studies for solving or reconstructing equations dealing with noise

is PINNs based on Bayesian methods. However, these studies require probabilistic modeling of noises, i.e., it requires assumptions about the likelihood. The current works usually assume Gaussian noise and do not consider anomalous data of unknown distribution. Some enlightening works are closely related to this paper among the deterministic approaches. Wang et al.[26] doubted the plausibility of L_2 loss and noticed the impact of loss functions on training PINN. Therefore, they used L_∞ -norm to penalize the collocation points with more significant residuals in the PDE term or boundary condition term and used these points as adversarial samples for accelerating training. In contrast, our paper assumes that there may be unreliable observations and adopts the L_1 -norm to reduce the impact of these outliers. Of course, these two methods are not mutually exclusive, where the L_1 -norm can be used in the data loss term while the L_∞ -norm can be used in the PDE loss term. [27] reconstructs the dynamics from highly corrupted observations in the dynamical system, and they also used the L_1 -norm to deal with unreliable observations. However, their model is essentially a sparse generalized linear model, while the PINN used in this paper is highly nonlinear, resulting in substantial differences in modeling and solving. Peng et al.[28] mentioned examples of robust coefficient recovery by employing the L_1 norm, but they lacked a more comprehensive evaluation of the method. The present paper provides a systematic comparison of multiple scenarios for a variety of anomalous data as well as a two-stage framework for more accurate reconstruction.

The paper is organized as follows. In Section 2, the backgrounds of PINN and robust linear regression are first presented. Section 3 introduces the LAD-based robust PINN method and a two-stage framework. Section 4 compares the methods systematically through four experiments, including two examples with known PDE parameters for solution reconstruction and two examples with unknown PDE parameters for recovery. Section 5 summarizes the results and concludes the paper.

2. Preliminaries

This paper is mainly based on two fundamental techniques, one of which is PINN and the other is M-estimator derived from robust statistical analysis. These two techniques are briefly described in this section.

2.1. Physics informed neural networks

In this subsection, we present an brief overview of vanilla PINN (OLS-PINN) for recovering solutions and identifying unknown parameters of PDEs. The main goal is to approximate the solution u for the following differential equation:

$$\mathcal{N}(t, x, u; \lambda) = 0, \quad t \in [0, T], x \in \Omega,$$

where \mathcal{N} denotes a general differential operator that may consist of derivatives, linear terms, nonlinear terms, and possibly unknown parameters λ . x denotes a spatial vector, and t is a scalar about time.

Following the work[1] of Raissi et al., given some observed spatiotemporal data $\mathbf{D}_u = \{(t_i, x_i, u_i)\}$, we are concerned with two problems, one of which is to recover the solution u , and the other is to identify λ for the case of unknown parameters included. PINN employs a feedforward neural network \hat{u} as the surrogate for the solution. We consider \hat{u}_θ a classic fully-connected

neural network parameterized by θ . Define the residual networks, which share the same network parameters θ :

$$r_{pde}(t, x; \theta, \lambda) := \mathcal{N}(t, x, \hat{u}(t, x; \theta); \lambda),$$

where automatic differentiation techniques compute all derivatives.

The shared network parameters θ are trained by minimizing loss terms that penalize the residuals for not equaling zero:

$$L(\theta, \lambda) = \omega \cdot L_{pde}(\theta, \lambda) + L_u(\theta), \quad (\omega > 0) \quad (1)$$

where L_{pde} is the PDE loss term, L_u is the data loss term, and $\omega > 0$ is a user-defined weighting coefficient for PDE loss. The PDE loss term is approximated by sampling inside the domain Ω :

$$L_{pde}(\theta, \lambda) = \frac{1}{\#\mathbf{D}_{pde}} \sum_{(x,t) \in \mathbf{D}_{pde}} |r_{pde}(t, x; \theta, \lambda)|^2, \quad (2)$$

where \mathbf{D}_{pde} is the collocation set for enforcing strong forms of PDEs, and the operator $\#$ denotes the number of elements in a set. For OLS-PINN, the data loss term is constructed by measuring the difference between the predicted values and given labels with the squared l_2 -norm:

$$L_u(\theta) = \frac{1}{\#\mathbf{D}_u} \sum_{(x_i, t_i, u_i) \in \mathbf{D}_u} |\hat{u}(t_i, x_i; \theta) - u_i|^2,$$

where $\mathbf{D}_u = \{(t_i, x_i, u_i)\}$ may contain samples from initial conditions, boundary conditions, and noisy measurements. Finally, the solution \hat{u}_θ and the unknown PDE parameter λ are approximated by minimizing the total loss $L(\theta, \lambda)$:

$$\theta^*, \lambda^* = \arg \min_{\theta, \lambda} L(\theta, \lambda). \quad (3)$$

The minimization problem can be solved by the gradient descent method Adam [29] and a limited memory variant of BFGS optimizer(L-BFGS-B) [30].

2.2. $L1$ robust regression for linear models

We consider recovering PDE solutions and unknown parameters from highly corrupted data that may contain outliers. Since methods of handling atypical data are comprehensively studied in robust linear regression analysis, which deals with outliers in the dataset simultaneously with the fitting process. Robust linear regression analysis provides motivations and approaches, allowing us to speculate on similar problems in data-driven PINN-related tasks. We will use some of these concepts from robust linear analysis contexts. Therefore, this subsection will briefly introduce several robust M-estimators for robust linear regression that are closely related to this paper, and the proposed robust PINN is essentially an extension to the nonlinear fields in the sense of deep neural network models.

Given the observations (x_i, u_i) , $i = 1, \dots, n$, in order to understand how the responses u_i s are related to the covariates x_i s, linear models usually assume the following form:

$$u_i = x_i^T \theta + \varepsilon,$$

where $\theta \in \mathbb{R}^p$ is unknown and to be determined. For the Gaussian noise ε , choosing $\rho_i(\cdot) := \|\cdot\|^2$ is preferred since the estimator coincides with maximum-likelihood estimates with the assumption of independent normally distributed errors with 0 mean and equal variances. The deduced least squared form can be solved readily with well-understood linear numerical algebra methods [31]:

$$\theta^* := \arg \min_{\theta} \sum_{i=1}^n (u_i - x_i^T \theta)^2. \quad (4)$$

The Ordinary Least Square (OLS) estimator introduced above is not robust since the occurrence of even a single outlier can spoil the result completely [32].

By replacing the least squares criterion (4) with a more robust criterion, the M-estimate [33] of θ is

$$\theta^* := \arg \min_{\theta} \sum \rho_i \left(\frac{u_i - x_i^T \theta}{\hat{\sigma}} \right),$$

where the choice of ρ_i has a significant effect on the results, and $\hat{\sigma}$ is the scale estimate of the error. When $\rho_i = \|\cdot\|^2$, it becomes OLS. Consider other functions such as L_1 norm, Tukey's biweight function, or Huber's loss function. The schematic of the 4 loss functions is shown in Fig.1. The three methods other than OLS can usually handle outliers. The reason is that these methods give much less weight to large deviations. For more tens of robust estimator loss functions, please refer to [34].

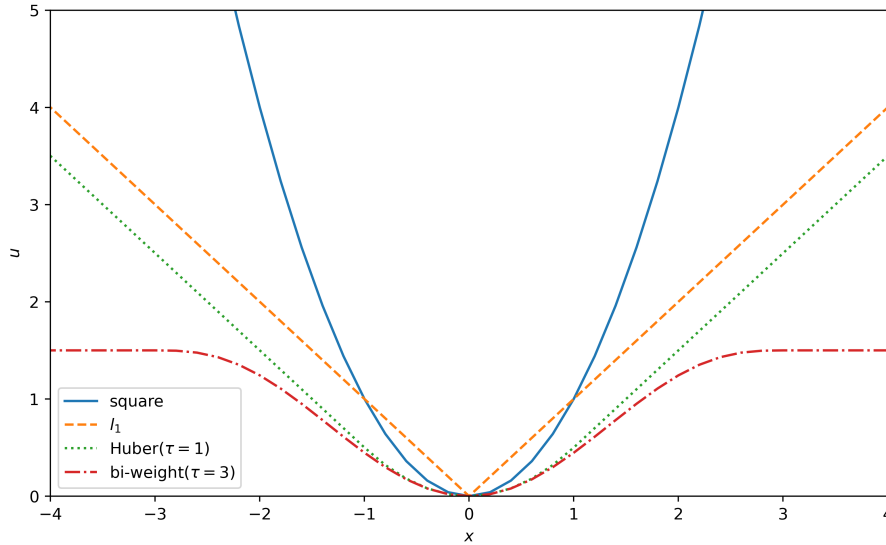


Figure 1: Different loss functions. Curve shapes of Huber's loss function and bi-weight are controlled by a hyperparameter τ . The square loss increases the fastest when $|x|$ becomes large.

In particular, the L_1 loss minimizes the sum of the absolute errors and is therefore also known as the Least Absolute Derivation (LAD) method:

$$\min_{\theta} \sum |u_i - x_i^T \theta|. \quad (5)$$

Although the LAD is inefficient in the robust linear regression context, i.e., LAD estimates have a low efficiency of 0.64 when the errors are distributed normally[33], LAD has the most straightforward form among all M-estimators and is straightforward for generalization. In the next section, we will use LAD to constrain the data items in PINN and illustrate the potential advantages and shortcomings of LAD compared to other M-estimators in PINN applications.

3. LAD Physics-Informed neural networks

Not only is OLS susceptible to outliers, but nonlinear models/neural networks may also be sensitive to outliers in datasets. For example, data poisoning attacks can cause specific neural network errors by adding spurious data to the training dataset [35]. In regards to the implementation of vanilla PINN, even one atypical observation can cause significant errors in the results (Fig.5). Therefore, motivated by the LAD method from robust linear analysis, we ameliorate this problem by minimizing the absolute value of the data discrepancy to handle possibly highly corrupted data. Then the PDE constrained optimization model is formulated as:

$$\begin{aligned} \min_{\theta, \lambda} \quad & \sum_{(t_i, x_i, u_i) \in \mathbf{D}_u} |u_i - u_\theta(t_i, x_i; \lambda)| \\ \text{s.t.} \quad & \mathcal{N}(t, x, u_\theta, \lambda) = 0, \end{aligned}$$

which is then transformed into the following unconstrained form:

$$\text{(LAD-PINN)} : \quad \min_{\theta, \lambda} \quad \frac{1}{\#\mathbf{D}_u} \sum_{(t_i, x_i, u_i) \in \mathbf{D}_u} |u_i - u_\theta(t_i, x_i; \lambda)| + \omega \cdot L_{pde}. \quad (6)$$

When the measurement u_i is a vector instead of a scalar, the data loss $\sum_i |e_i|$ extends to $\sum_i \|e_i\|_1$ or $\sum_i \|e_i\|_2$, which corresponds to the sparse regularization and the group sparse regularization [36], respectively. In our experiment involving vector measurements, we choose $\sum_i \|e_i\|_1$ as the data loss.

Eq.(6) replaces the squared term in Eq.(1) with the L_1 loss term. Note that the unconstrained model is not equivalent to the PDE constrained model. Indeed, if a physical law is only constrained approximately, the solution may exhibit a different quality or even reach a completely wrong answer. However, *All models are wrong, but some are useful* [37]. Since unconstrained optimization models are usually easier to be solved, Eq.(1) has been widely used in various fields along with the vanilla PINN. Therefore, the unconstrained LAD-PINN model (Eq.(6)) also promises to achieve satisfactory results.

From the perspective of solving a constrained optimization, using the penalty function method or the augmented Lagrange multiplier method seems to be more appropriate [34, 9, 38]. However, these two kinds of methods not only involve more hyperparameter selections but also require solving the minimization sub-problems several times. In order to reduce burdens in the endless algorithm hyperparameter selection, we insist on converting the PDE constraint into an unconstrained minimization form. The proposed method only needs to select one hyperparameter at the modeling level and solve the minimization problem only once.

In Eq.(6), we are trying to minimize the absolute derivations instead of squared errors. Similar to LAD used in robust linear regression, one can deduce that the L_1 norm loss function is less likely to be affected by outliers compared to the squared l_2 norm that is employed in vanilla

PINN. Hence, the impact of a significant deviation of observed data from predicted values has been greatly diminished.

Among the various methods of robust linear analysis, although the M-estimator LAD has only a breakdown point and a low efficiency of 0.64 when the errors are distributed normally [32], it is free from additional hyperparameter selection. Since training a PINN is usually much more expensive than solving a linear model. Currently, we may not have an efficient way to select hyperparameters and evaluate them. Therefore, in this paper, LAD is chosen to be combined with PINN. In addition, it is also popular to use the L_1 loss term for weight regularization in deep neural networks, and thus the corresponding available optimizer for the non-smooth problem seems more applicable to LAD-PINN than the models deduced from other delicate robust estimators.

3.1. LAD-PINN as an abnormal detector: a two-stage framework

Data cleaning is a mandatory step in the usual data-driven tasks. Although LAD-PINN completes both anomalous data processing and subsequent training tasks simultaneously, we can use LAD-PINN only for data cleaning to get a relatively clean data set. LAD-PINN can usually recover stable results from highly corrupted data, but due to the lower efficiency of LAD relative to OLS, the accuracy of LAD-PINN is usually lower than vanilla PINN in the noiseless or low standard Gaussian noise cases, which may result in the failures in revealing hidden physics (subsection 4.2.1 and subsection 4.4.1).

Referring to the idea of the iterative robust regression analysis methods such as REWLSE[39] or RANSAC[25] which gradually eliminates anomalies through a multi-stage approach, considering the iterative multi-stage might bring heavy computational burdens for training PINN, we propose a two-stage training method in moderation.

In the first stage, the target physical field is stably reconstructed by LAD-PINN under potentially highly corrupted data. LAD-PINN works as an anomaly detector, and its predicted field is regarded as a reference to identify outliers based on the distribution of the difference between observed and predicted values in the dataset. The identified data points are removed to obtain a cleaned dataset. The physical field is then reconstructed in the second stage based on the cleaned dataset using OLS-PINN. The network trained by LAD-PINN in the first stage is also used as a pre-trained network to help accelerate the training of the second stage. This two-stage framework is described by Alg.1.

The two minimization problems in Line 1 and Line 3 in Alg.1 are solved following the routines of PINN. Various acceleration techniques can also be integrated into the framework, including but not limited to the improvements in the introduction.

Line 2 detects and filters the abnormal data. Suppose the original dataset is $\mathbf{D}_u = \{(t_i, x_i, u_i)\}$ and the set of corresponding predicted values obtained using the LAD-PINN model is $\mathbf{D}_p = \{t_i, x_i, \hat{u}^+(t_i, x_i)\}$. Outliers are determined by comparing the differences between the two data sets, i.e., $\{t_i, x_i, \hat{u}^+(t_i, x_i) - u_i\}$. Accuracy of this approach may heavily depend on knowledge of the prior error distribution, and accurate priors may significantly enhance the results. Here we provide two approaches in the absence of specific priors.

In the first approach, the points corresponding to a certain percentage k of the maximum absolute errors are designated anomalies and removed. This approach is simple and may be very effective especially if there is an accurate prior for the proportion. Otherwise, when the proportion k is chosen too large, the normal data with an acceptable scale of noises may be removed mistakenly, and these removed normal data may be concentrated on a poorly trained

Algorithm 1 A two-stage robust PINN framework

Require: Dataset with possibly highly corrupted observations: $\mathbf{D}_u = \{(t_i, x_i, u_i)\}$

PDE: $\mathcal{N}(t, x, u; \lambda) = 0$

Filter parameter: k

- 1: The first stage training by LAD-PINN;

$$\hat{u}^+, \lambda^+ \leftarrow \arg \min_{\hat{u}, \lambda} \frac{1}{\#\mathbf{D}_u} \sum_{(t_i, x_i, u_i) \in \mathbf{D}_u} |\hat{u}(t_i, x_i) - u_i| + \omega \cdot \|\mathcal{N}(t, x, \hat{u}; \lambda)\|_2^2 \quad (7)$$

- 2: Screening out the highly corrupted data with large $|\hat{u}^+(t_i, x_i) - u_i|$;

$$\hat{\mathbf{D}}_u \leftarrow \text{Filter}(\mathbf{D}_u, \hat{u}^+; k) \quad (8)$$

- 3: The second stage training by OLS-PINN;

$$\hat{u}^*, \lambda^* \leftarrow \arg \min_{\hat{u}, \lambda} \frac{1}{\#\hat{\mathbf{D}}_u} \sum_{(t_i, x_i, u_i) \in \hat{\mathbf{D}}_u} |\hat{u}(t_i, x_i) - u_i| + \omega \cdot \|\mathcal{N}(t, x, \hat{u}; \lambda)\|_2^2 \quad (9)$$

return \hat{u}^*, λ^*

region, resulting in an observation hole, as Fig.11(d) shows. When the proportion k is chosen too small, the small amount of remaining abnormal data can also cause the subsequent OLS-PINN to fail due to its high sensitivity to outliers.

Another approach is to assume that the differences $\{u_i - \hat{u}^+(t_i, x_i)\}$ of non-outliers obey a normal distribution. We estimate the standard deviation of the distribution by median absolute deviation (MAD) and use the standard deviation to construct a threshold to exclude the outliers. The idea of MAD was (re-)discovered and popularized by [40]. Since the MAD estimation is very robust with a breakpoint of 50% [41], the variance of the normal distribution can be estimated in a highly corrupted dataset to screen out the outliers. Specifically, the estimated standard deviation is

$$\hat{\sigma}_e = \frac{1}{1.6777} \cdot \text{median}(|u_i - \hat{u}^+(t_i, x_i)|).$$

If u_i lies in the neighborhood $\{u \mid |\hat{u}^+(t_i, x_i) - u| \leq k \cdot \hat{\sigma}_e\}$, the point is reserved; otherwise, it is identified as abnormal and removed. k is usually chosen as 2.0, 2.5 or 3.0 [41]. Subsequent experiments have shown that the method is not sensitive to k , and similar results can be obtained for all three common choices.

In the paper, the combination of Adam and L-BFGS-B is used for the first stage, and the second stage can be accelerated by using the pre-trained \hat{u}^+ in the first stage as an initialization. In the second stage of training, several steps with a large learning rate are first applied for regularization [42], which can avoid falling into the local optimal obtained by the first stage, although it may temporarily reduce the accuracy of the model.

4. Experiments

In the numerical experiments, we consider two types of problems separately: whether the controlling PDE contains unknown parameters.

First, we consider the problems of recovering the physical field under incomplete boundary conditions with known PDE parameters, which include solving the one-dimensional Poisson's equation and two-dimensional steady Navier-Stokes (N-S) equations. Then we consider problems containing unknown PDE parameters, including a one-dimensional wave equation and two-dimensional unsteady N-S equations. In particular, we reconstruct the hidden pressure fields using the two-stage algorithm (Alg.1) in the two N-S equation problems.

The noisy data is generated by:

$$u_i := \hat{u}_i + \varepsilon_i$$

where \hat{u}_i is extracted from reference solutions, which are regarded as exact. Furthermore, we consider noise terms ε_i from different random distributions.

The following kinds of data corruption [43] are considered in the experiment, including noises obeying Gaussian distribution, mixed Gaussian distribution, Cauchy distribution, and fixed spurious values in the u_i . We presume that for the reference u to be corrupted, a scaling factor is first defined as $\hat{\sigma} = \text{std}(u)$. To facilitate a uniform description of the different data corruption types, assume the corrupted level $\alpha \in (0, 1)$ for all types. Specifically, five corruption classes are employed:

1. **Gaussian:** Noises obey normal distribution, i.e., $\varepsilon_i \sim \mathcal{N}(0, \alpha^2 \hat{\sigma}^2)$, the standard derivation of which is $\alpha \cdot \hat{\sigma}$.
2. **Contaminated:** The noises obey Gaussian mixed distribution, generating a large number of Gaussian noise data with small variance and a small number of Gaussian noise data with significant variance, i.e., $\varepsilon \sim 0.8 \cdot \mathcal{N}(0, \alpha^2 \hat{\sigma}^2) + 0.2 \cdot \mathcal{N}(0, (10\alpha\hat{\sigma})^2)$. The standard derivation is $4.64\alpha\hat{\sigma}$. To reduce the simulation variance, we fix the ratio of noisy data from the two Gaussian distributions, and thus the noises are not independent.
3. **Cauchy:** The noises obey the Cauchy distribution:

$$\varepsilon \sim \frac{1}{\pi\alpha\hat{\sigma}(1 + \frac{x^2}{\alpha^2\hat{\sigma}^2})} \quad (10)$$

the variance of which is undefined.

4. **Outlier:** Set $100\alpha\%$ of the observations u_i to a fixed spurious value. Unlike the several noises above, this data corruption is asymmetric,
5. **Mixed:** Set $100\alpha\%$ of the observations u_i to a fixed spurious large value (10 or 30). The noises that obey the normal distribution $\mathcal{N}(0, \alpha^2 \hat{\sigma}^2)$ are added to the rest of the observations.

The different distribution probability density functions corresponding to the several kinds of noise are shown in Fig.2. The heavy tail usually means that noises are prone to large derivation.

All numerical experiments are mainly based on Tensorflow and other open-source Python packages. The fully connected MLP is employed in all experiments. The activation function is *tanh*, and the rest of the detailed configurations are described in the respective experiment. Unless otherwise specified, the error in the experiments is defined by the relative l_2 error, i.e.,

$$\text{RE}(\hat{u}) = \frac{\|\hat{u} - u\|_2}{\|u\|_2}. \quad (11)$$

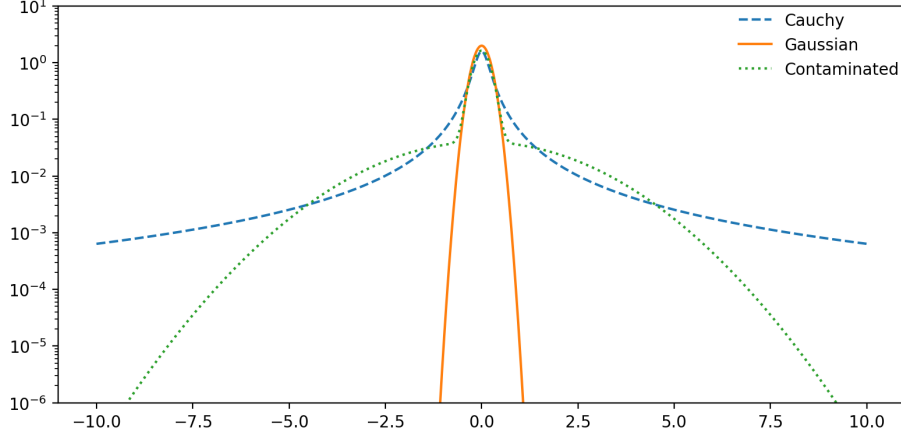


Figure 2: Probability distribution functions corresponding to different noise types. The Cauchy and mixed Gaussian distributions are more prone to produce highly corrupted data.

PDE	Unknown Parameters	Layers	Adam iterations	Two-stage
Poisson	No	[1,50,50,50,50,1]	15000	No
Steady N-S	No	[2,40,40,40,40,40,40,40,5]	10000	Yes
Wave	Yes	[2,40,40,40,40,1]	10000	No
Unsteady N-S	Yes	[3,20,20,20,20,20,20,20,20,2]	10000	Yes

Table 1: Configurations for each experiment: The *Unknown Parameters* column indicates if there is unknown parameters in the controlling PDEs. The *Layers* column describes the neuron numbers used in each layer of a neural network. The *Adam iterations* column tells the maximum number of Adam iterations. The *Two-stage* column shows whether the two-stage framework is employed in the experiment.

Configurations for the four experiments are listed in Tab 1.

4.1. One-dimensional Poisson's equation

The first experiment considers a simple one-dimensional Poisson's equation:

$$u_{xx} = -16 \sin(4x). \quad (12)$$

Assume that the ground truth is $u(x) = \sin(4x) + 1$. Observations are sampled from the interval $[-\pi, -\pi/2]$ and the solution on the interval $[-\pi, \pi]$ is to be reconstructed.

First, we clarify that it is almost impossible to recover the solution on interval $[-\pi, \pi]$ based on observations from $[-\pi, 0]$ without physical constraints. When a neural network is applied for fitting, the results is shown in Fig. 3. In the absence of embedding physical priors, the neural network has no generalization ability in the sense of physical laws and cannot learn a correct solution on $[-\pi, \pi]$. On the other hand, for noisy data, the neural network under sufficient training will overfit the data. Integrating the PDE loss can solve both problems as shown in Fig.4.

Therefore, it is necessary to consider PDE loss in such regression or reconstruction tasks. Denote \hat{u} the computed solution approximated by a neural network:

$$\hat{u}(x) = \text{net}(x). \quad (13)$$

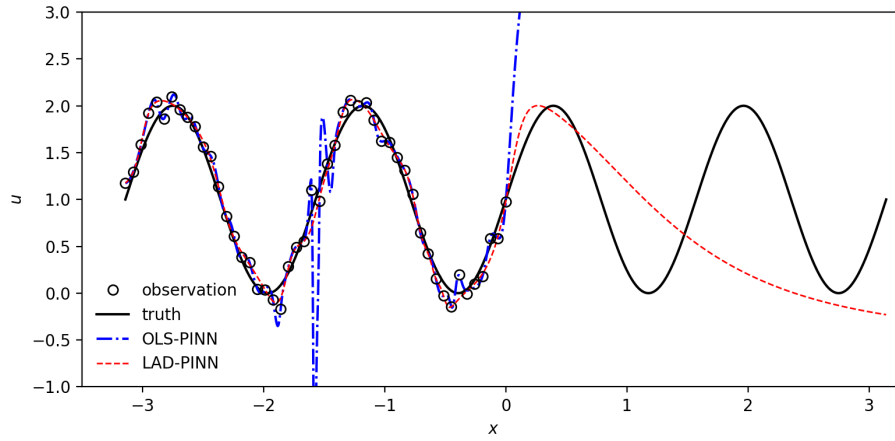


Figure 3: Regression without physics-informed regularizers. It can be challenging to generalize outside the observations, as there is no guarantee that the NN model has learned the relevant physics. OLS-NN overfits the noisy observations apparently.

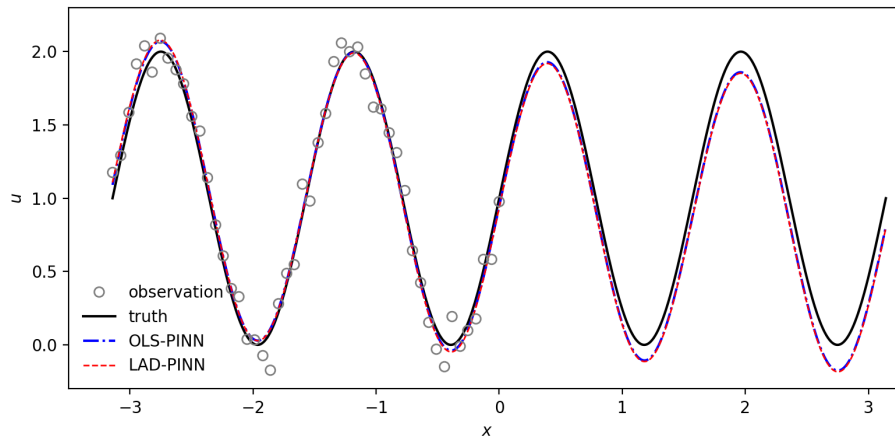


Figure 4: Nonlinear regression with physics-informed regularization, i.e., PINN. When the PDE loss term is integrated, both LAD-PINN and OLS-PINN learn the solution successfully.

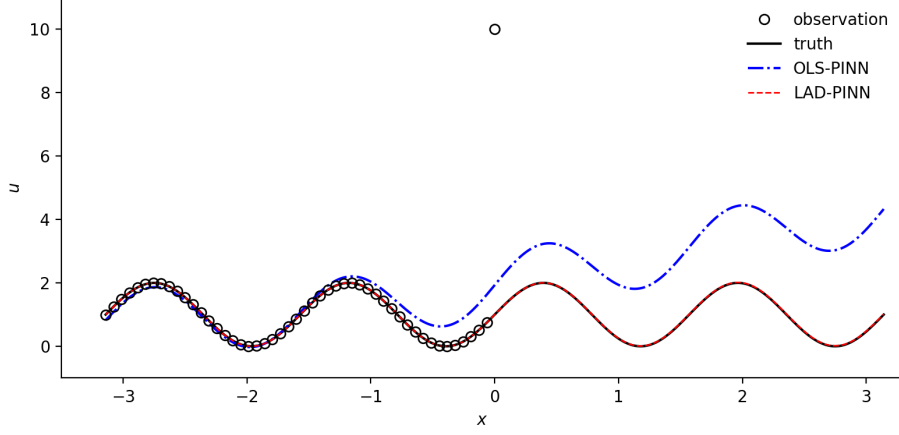


Figure 5: Observations with a single outlier in the u -direction. LAD-PINN succeed to recover the solution while OLS-PINN biases the result.

Then the unconstrained optimization model is approximated on collocation points and observations:

$$L := \omega \cdot \frac{1}{\#\mathbf{D}_{pde}} \sum_{x_i \in \mathbf{D}_{pde}} |\hat{u}_{xx}(x_i)|^2 + \frac{1}{\#\mathbf{D}_u} \sum_{(x_i, u_i) \in \mathbf{D}_u} |\hat{u}(x_i) - u_i| \quad (14)$$

For the one-dimensional time-independent problem (12), the general solution is

$$u(x) = \sin(4x) + ax + b. \quad (15)$$

If the observations are free of noise, only two different data points on the interval can determine the solution, and thus the solution can be recovered exactly. Therefore, only the data corruption cases are considered in the experiment.

Taking $\omega = 1.0$, the number of observations is 1,000 and the fixed number of iterations is 15,000 Adam steps, followed by an L-BFGS-B optimizer. The results are shown in Tab.2. There is an increase in the resultant error as the corruption level rises. Under Gaussian noise, the performance of LAD-PINN and OLS-PINN are similar, but for the case of Contaminated, Cauchy and Outliers, LAD-PINN has an advantage in accuracy, and for the cases containing spurious data in the u -direction, OLS-PINN can hardly reconstruct correctly.

Fixing the corruption level α to be 0.2, we vary the number of given observations. As is shown in Tab.3, OLS-PINN cannot recover the solution with spurious values in the u -directions. Instead, LAD-PINN recovers all the solutions. Furthermore, LAD-PINN achieves better accuracy expect for the Gaussian noises, which is consistent to the high-efficiency of OLS and robustness of LAD in robust linear analysis.

The choice of weights have an impact on the results. As shown in Fig.6, a fixed weight $\omega = 1.0$ is a suitable choice for LAD-PINN with various data corruption. The weight is also suitable for OLS-PINN with clean data or Gaussian noise. However, OLS-PINN fails for all weights in the cases containing outliers.

α	Loss	Gaussian	Contaminated	Cauchy	Outlier	Mixed
0.10	LAD	0.618	1.702	2.155	0.029	2.851
	OLS	0.658	4.763	5.706	108.798	108.691
0.15	LAD	0.700	1.712	2.711	0.316	3.097
	OLS	0.784	7.235	8.409	146.125	146.089
0.20	LAD	0.821	1.628	2.758	0.411	4.018
	OLS	1.150	9.586	11.505	160.362	159.951
0.25	LAD	0.953	1.521	2.895	0.099	6.197
	OLS	1.409	11.692	14.421	197.860	197.699
0.30	LAD	1.122	1.539	3.022	0.187	9.035
	OLS	1.698	14.366	17.163	213.080	213.321

Table 2: Relative errors(%) of the solution u to the Poisson's equation with different corruption levels for $\#\mathbf{D}_u = 500$.

$\#\mathbf{D}_u$	Loss	Gaussian	Contaminated	Cauchy	Outlier	Mixed
100	LAD	11.482	11.374	1.783	0.168	5.983
	OLS	4.777	14.744	29.090	112.737	112.755
200	LAD	1.478	12.855	3.405	0.292	3.290
	OLS	1.772	28.526	72.338	221.448	218.376
300	LAD	0.568	0.639	3.375	0.823	6.595
	OLS	0.999	5.779	20.494	197.473	197.046
400	LAD	3.293	2.802	1.252	1.034	3.259
	OLS	3.222	7.912	5.297	141.417	138.910
500	LAD	0.821	1.628	2.758	0.732	4.159
	OLS	1.150	9.586	11.505	160.334	159.656

Table 3: Relative errors(%) of the solution u to the Poisson's equation with different dataset sizes for $\alpha = 0.2$.

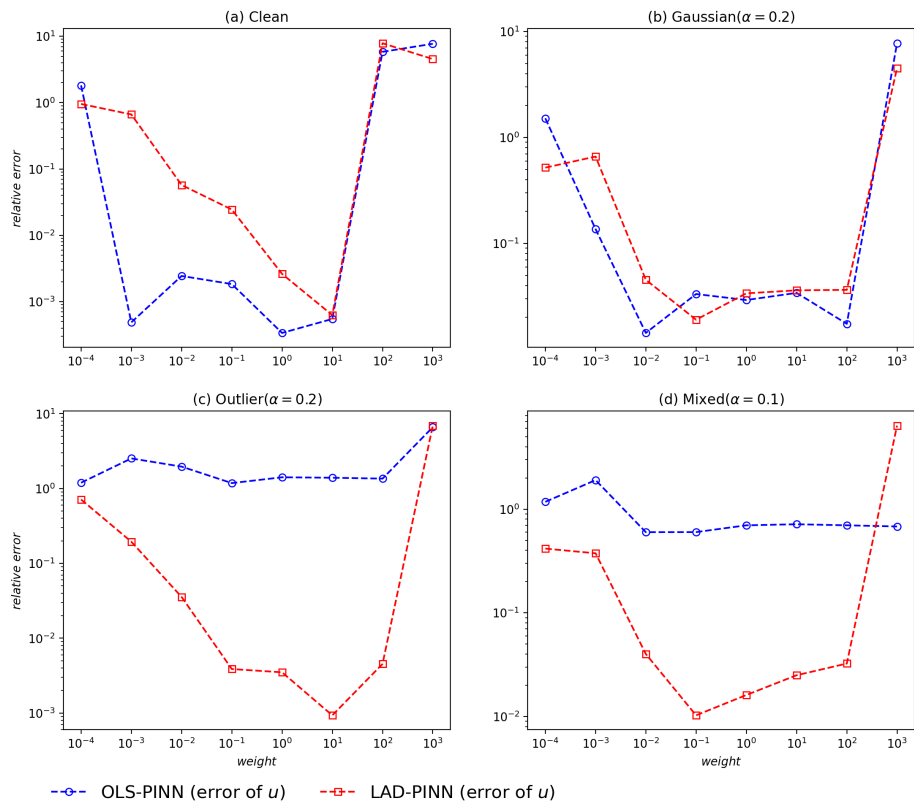


Figure 6: Effects of the weight parameter ω under different corruption types for the Poisson's equation. ($\#\mathbf{D}_u = 400$, $\alpha = 0.2$)

4.2. Steady 2D N-S equations

The Navier-Stokes equations describe the physics of many phenomena in science and engineering, which can be used to model weather, ocean currents, fluids in pipes and airflow around airfoils. This subsection considers a two-dimensional steady-state Navier-Stokes equations describing laminar flow, with the underlying equation given by

$$uu_x + vu_y = -p_x + u_{xx} + u_{yy} \quad (16)$$

$$uv_x + vv_y = -p_y + v_{xx} + v_{yy} \quad (17)$$

where $u(x, y)$ denotes the x-component of the velocity field, $v(x, y)$ the y-component, and $p(x, y)$ the pressure. Incompressible solutions to the equations are constrained by the continuity equation:

$$u_x + v_y = 0, \quad (18)$$

which describes the conservation of mass of the incompressible fluid.

The prototype problem of incompressible flow past a circular cylinder is considered. In this work, we reuse numerical example released by Rao et al.[44]. An observation in the dataset is a quadruple (x_i, y_i, u_i, v_i) , where the pressure is hidden from measurements. The profile is shown in Fig.7.

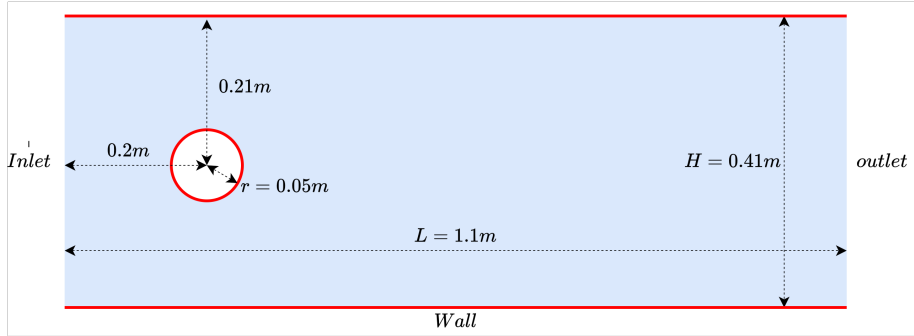


Figure 7: Problem setup of the steady N-S equation experiment. The profile of flow around a circular cylinder follows [44]. The red represents walls with the no-slip condition. We assume that the inlet boundary condition is unknown to the algorithm in the experiment.

The velocity vector is set to zero at all walls and the pressure is set to $p = 0$ at the outlet. The fluid density is taken as $\rho = 1kg/m^3$ and the dynamic viscosity is taken as $\mu = 2 \cdot 10^{-2}kg/m^3$. The velocity profile on the inlet is set as

$$u(0, y) = 4 \frac{U_M}{H^2} (H - y)y$$

with $U_M = 1m/s$ and $H = 0.41m$. Note that the inlet profile is unknown to the algorithm, and thus we need to recover the flow fields with the incomplete boundary conditions.

To illustrate the generalization performance of the presented method, we exactly follow the network architecture proposed by Rao et al.[44], where the Cauchy stress tensor σ is introduced to reduce the order of derivatives in PINN.

Therefore, Eq.(16) and Eq.(18) is equivalently transformed into the following equations:

$$\begin{aligned}
\sigma^{11} &= -p + 2\mu u_x \\
\sigma^{22} &= -p + 2\mu v_y \\
\sigma^{12} &= \mu(u_y + v_x) \\
p &= -\frac{1}{2}(\sigma^{11} + \sigma^{22}) \\
(uu_x + vv_y) &= \mu(\sigma_x^{11} + \sigma_y^{12}) \\
(uv_x + vv_y) &= \mu(\sigma_x^{12} + \sigma_y^{22})
\end{aligned}$$

We construct a neural network with six outputs to satisfy the PDE constraints above:

$$u, v, p, \sigma^{11}, \sigma^{12}, \sigma^{22} = net(x, y) \quad (19)$$

Samples from known boundary conditions are regarded as observations which are always clean. Combining the PDE constraints, boundaries conditions and observations, we obtain a total loss like Eq.1 or Eq.6.

First we consider the noiseless case, where u, v are recovered accurately, as shown in Fig.8. However, once a small number of outliers are added to the dataset, OLS-PINN collapses while

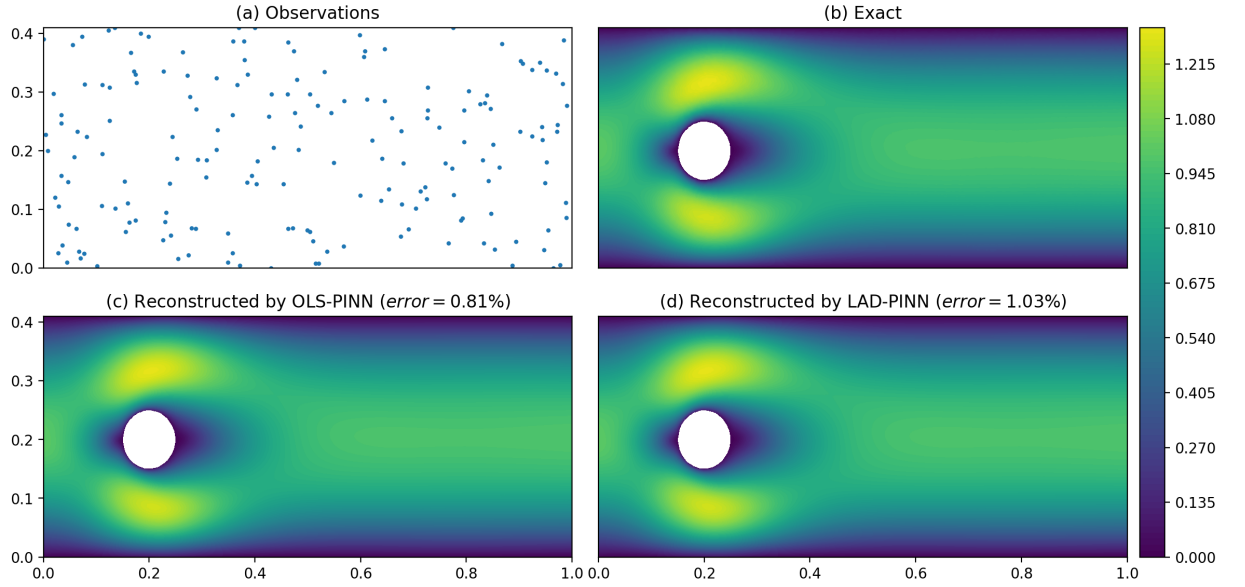


Figure 8: Magnitude of reconstructed velocity with sparse clean data. Observations are randomly located in the domain as (a) shows. Both OLS-PINN (c) and LAD-PINN (d) reach a precise reconstruction with the observations.

LAD-PINN can still reconstructed the velocity field, as shown in Fig.9. For a systematic comparison, 200, 400, 600, 800, and 1000 points in the computational domain are randomly selected as observations, respectively. The results under different types of data corruption is shown in Tab.4, where the corruption level α is fixed to 0.2. In this experiment, the relative errors of LAD-PINN

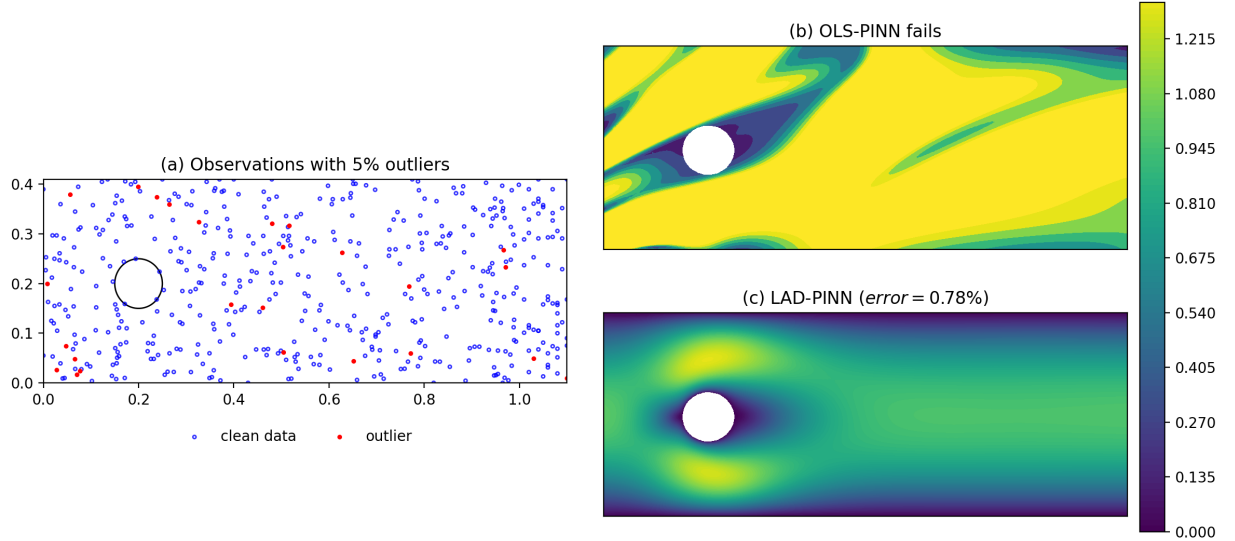


Figure 9: Observations corrupted by 5% spurious values in velocity. The 5% outliers in the dataset are marked solid red (a). The OLS-PINN fails (b) while LAD-PINN reconstructs the velocity field even with the outliers (c).

tend to decrease as the number of observations increases. The results under different levels of data corruption is shown in Tab.5, where the number of observations is fixed to 1000. The accuracy of LAD-PINN tends to decrease as the corruption level increases. In both experiments, except for the Gaussian case, the results of LAD-PINN are better than OLS-PINN for other data corruptions, which are consistent with the results for LAD and OLS in robust linear analysis.

4.2.1. Reveal pressure via the two stage algorithms

Setting $\alpha = 0.2$ and $\#\mathbf{D}_u = 500$, we compare the two-stage PINN framework implemented by different filter strategies and filter parameters. The result is shown in Tab.6. LAD-PINN fails to recover the pressure field with high precision. OLS-PINN collapses when highly corrupted data are involved. Except for FR(0.1), other two-stage methods recover the pressure field in relatively high accuracy ($RE < 5\%$). The data sizes used in the second stage is also shown in the table, where MAD-PINN has small changes in the size. The reconstructed pressure around the cylinder is shown in Fig.10, where MAD-PINN(0.2) achieves an acceptable recovery.

In Tab.6, FR-PINN(0.1) collapses under the cases where spurious values are involved, the reason for which is as follows. If the FR approach is used, the three situations in Fig.11 may occur. When there is no accurate prior about the proportion of outliers, setting the proportion too small may cause the outliers to remain in the data set, and in Fig.5 we have found that a small number of outliers is enough to make OLS-PINN in the second stage collapse. On the other hand, if the proportion is set too high, all the “normal” data points in a small region are removed, creating a hole in the observations. As shown in Figure 12, MAD-PINN is not sensitive to common filter parameters(2.0, 2.5, 3.0), which does not removes too many normal points while excludes all outliers. No corruption level priors are needed, so it also indicates that the MAD-PINN may have better generalizability in practice.

# \mathbf{D}_u	Loss	Gaussian	Contaminated	Cauchy	Outlier	Mixed
200	LAD	3.468	7.974	9.978	5.212	6.608
	OLS	2.161	12.586	44.884	554.136	560.264
400	LAD	2.957	3.642	4.724	2.880	7.485
	OLS	2.013	12.129	43.523	510.407	525.471
600	LAD	2.290	3.041	3.436	0.963	6.208
	OLS	1.776	7.940	43.111	478.800	475.587
800	LAD	2.187	2.805	3.154	2.307	2.302
	OLS	1.553	5.526	42.126	475.588	471.305
1000	LAD	1.910	1.916	2.966	0.787	2.183
	OLS	1.370	4.745	56.682	466.165	464.685

Table 4: Relative errors(%) of reconstruct velocity fields to the steady N-S equation with different dataset sizes for $\alpha = 0.2$.

α	Loss	Gaussian	Contaminated	Cauchy	Outlier	Mixed
0.10	LAD	1.031	1.004	1.453	0.644	1.361
	OLS	0.826	2.260	23.313	341.776	341.837
0.15	LAD	1.298	1.400	2.026	2.301	4.341
	OLS	0.975	3.278	28.110	470.652	487.332
0.20	LAD	1.690	1.647	2.567	1.975	5.127
	OLS	1.209	4.357	34.447	598.716	600.624
0.25	LAD	2.022	1.900	2.825	4.244	5.681
	OLS	1.416	5.431	47.418	724.751	753.525
0.30	LAD	2.324	2.362	3.294	5.476	7.311
	OLS	1.710	6.917	53.805	851.395	850.893

Table 5: Relative errors(%) of reconstructed velocity fields to the steady N-S equation with different corruption levels for $\#\mathbf{D}_u = 1000$.

name		clean	Gaussian	Contaminated	Cauchy	Outlier	Mixed
LAD	RE(%)	9.613	11.263	11.410	8.143	60.218	60.335
	# $\hat{\mathbf{D}}_u$	500	500	500	500	500	500
OLS	RE(%)	3.086	4.676	9.805	76.335	407.450	587.055
	# $\hat{\mathbf{D}}_u$	500	500	500	500	500	500
FR(0.1)	RE(%)	3.451	4.285	5.538	2.757	958.879	869.857
	# $\hat{\mathbf{D}}_u$	450	450	450	450	450	450
FR(0.2)	RE(%)	3.223	4.037	4.483	3.346	3.012	4.407
	# $\hat{\mathbf{D}}_u$	400	400	400	400	400	400
FR(0.3)	RE(%)	3.466	4.286	4.882	3.084	3.062	4.430
	# $\hat{\mathbf{D}}_u$	350	350	350	350	350	350
MAD(2.0)	RE(%)	3.686	4.342	4.614	2.708	3.106	4.180
	# $\hat{\mathbf{D}}_u$	440	474	401	381	327	389
MAD(2.5)	RE(%)	3.198	4.758	4.995	3.329	3.219	4.420
	# $\hat{\mathbf{D}}_u$	460	493	414	399	340	391
MAD(3.0)	RE(%)	3.290	4.672	4.795	3.047	3.258	4.119
	# $\hat{\mathbf{D}}_u$	472	498	422	420	346	395

Table 6: Relative errors(%) of the reconstructed pressure p in the steady N-S equation for $\#\mathbf{D}_u = 500$ and $\alpha = 0.2$: Bold numbers highlight the case with the best error for each corruption type.

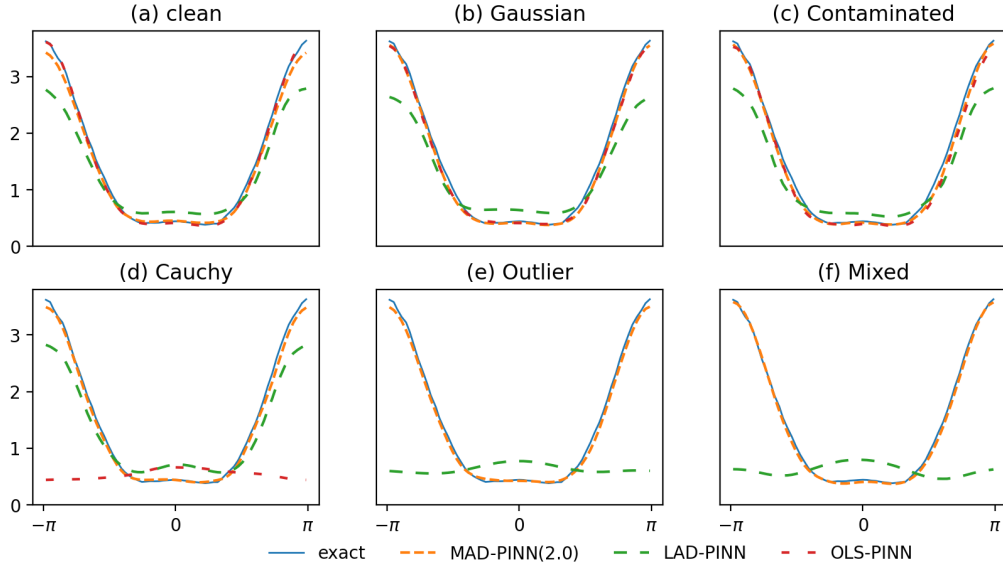


Figure 10: Reconstructed pressure around the cylinder for different corruption types. The red dash curves for OLS-PINN does not appear in (e) and (f) due to the results fall out of the displayed ranges.

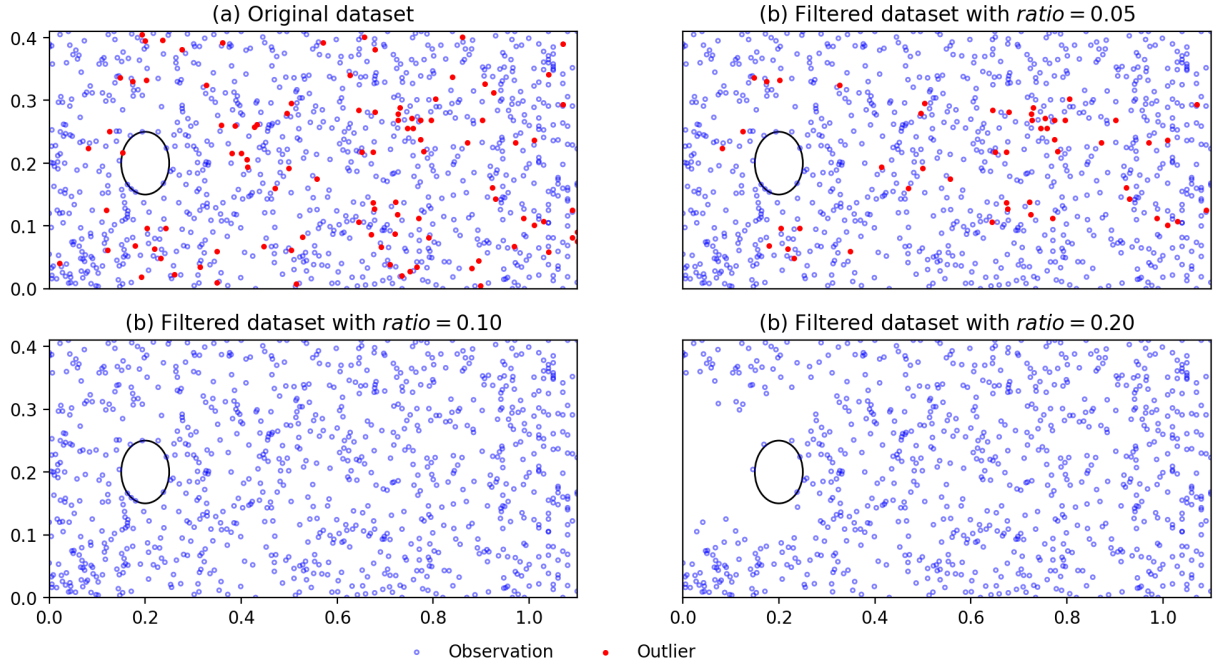


Figure 11: Different filter parameters for FR. (b) When the filter ratio is too small, the spurious values will remain in the dataset. (d) When the filter ratio is too large, all the *normal* points in a small region are removed, which results in a hole without any observations near the inlet.

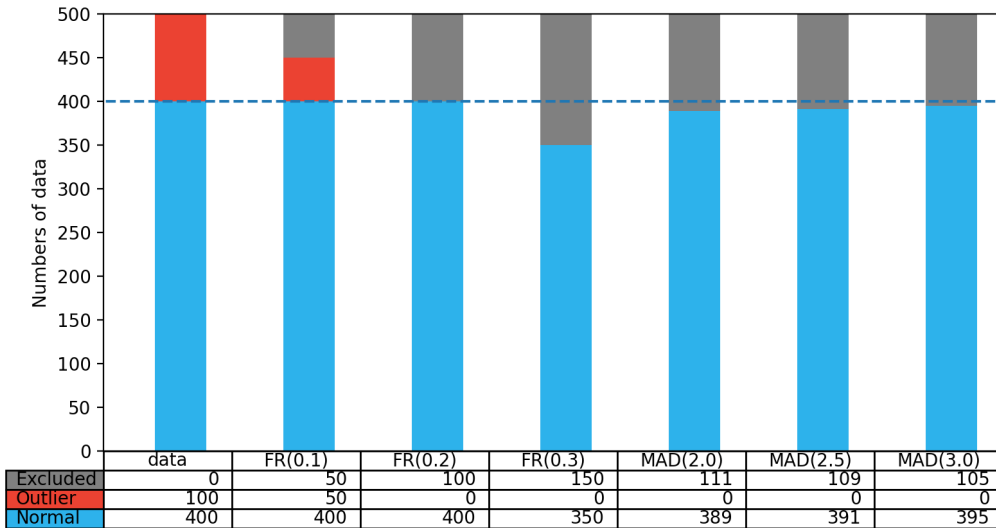


Figure 12: Composition of the observations employed in the second stage for different methods. The first column shows the observations are impaired by the Mixed corruption ($\alpha = 0.2$). The second column shows that FR-PINN(0.1) fails to remove all the spurious values. The last three column show that the dataset sizes remain stable for MAD-PINN with three different filter parameters.

4.3. One-dimensional wave equation with unknown parameters

In this example, we consider the one-dimensional wave equation with a unknown parameter:

$$u_{tt} = c \cdot u_{xx}, \quad (t, x) \in \Omega = [0, 2\pi] \times [0, \pi], \quad (20)$$

where the parameter $c = 1.0$ is assumed to be unknown. The ground truth is

$$u = \sin x \cdot (\sin \sqrt{c} \cdot t + \cos \sqrt{c} \cdot t). \quad (21)$$

In this problem, we only have limited noisy data and the PDE constraint (20) without any boundary or initial conditions. The Adam optimizer is applied to both the neural network parameters and the PDE parameter c in the iterations. The ground truth is illustrated in Fig.13. Fig.14 shows

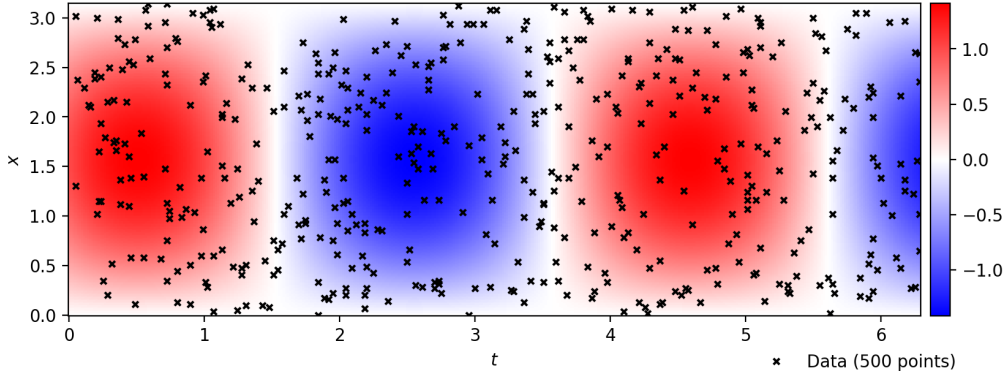


Figure 13: The ground truth of the wave equation and observations. 500 observations are randomly sampled in the interior of the domain Ω .

250 observations corrupted by Gaussian noise ($\alpha = 0.2$).

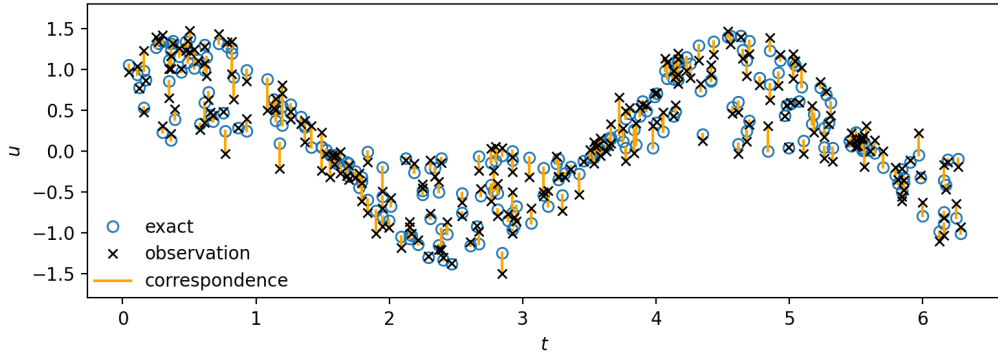


Figure 14: The exact values and the corresponding corrupted observations projected onto the t - u plane. 250 random points are corrupted by 20% uncorrelated Gaussian noise.

To further scrutinize the performance of the proposed method, we have performed a systematic study with respect to the size of observation dataset, the corruption levels and the weight of

# \mathbf{D}_u	loss	Clean	Gaussian	Contaminated	Cauchy	Outlier	Mixed
200	LAD	2.492	5.402	6.084	14.699	3.169	7.987
	OLS	0.495	11.244	255.549	118.851	497.638	554.716
400	LAD	0.707	3.341	4.252	4.442	1.622	4.353
	OLS	0.362	2.384	261.212	82.617	368.784	377.041
600	LAD	0.429	2.684	3.055	3.936	0.600	3.211
	OLS	0.109	2.104	174.771	323.152	274.044	273.428
800	LAD	0.692	2.211	2.496	2.853	0.504	2.953
	OLS	0.191	1.967	169.544	317.465	211.707	213.715
1000	LAD	0.565	2.086	2.456	3.090	1.766	2.595
	OLS	0.127	1.513	135.489	251.246	314.845	303.172

Table 7: Relative errors(%) of the solution u to the wave equation with different dataset sizes for $\alpha = 0.1$.

# \mathbf{D}_u	loss	Clean	Gaussian	Contaminated	Cauchy	outlier	mixed
200	LAD	4.362	6.615	4.842	14.399	9.231	9.251
	OLS	2.517	2.625	52.035	80.788	97.263	93.979
400	LAD	3.087	2.146	1.161	3.920	5.217	3.783
	OLS	2.561	0.613	85.672	8.559	69.222	71.760
600	LAD	2.962	2.672	2.933	2.431	2.632	3.040
	OLS	2.526	2.898	53.954	42.297	52.241	52.404
800	LAD	2.604	2.029	3.199	2.344	2.359	3.128
	OLS	2.546	2.602	57.855	69.769	33.706	32.523
1000	LAD	2.867	2.303	2.779	1.804	3.613	3.481
	OLS	2.550	2.814	37.539	35.793	98.799	98.314

Table 8: Relative errors(%) of the recovered parameter c in the wave equation with different dataset sizes for $\alpha = 0.1$.

the PDE loss term. First, 200, 400, 600, 800, and 1000 points in the computational domain are randomly selected as observations, respectively. The results for u and c under different types of data corruption is shown in Tab.7 and Tab.8, where the corruption level α is fixed to 0.1. The results under different levels of data corruption is shown in Tab.9 and Tab.10, where the number of observations is fixed to 1000. In the clean cases, OLS-PINN performs better than LAD-PINN. In the Gaussian cases, OLS-PINN is comparable with LAD-PINN. For the remaining highly corrupted cases, OLS-PINN usually has large errors or even crashes. The results of LAD-PINN are more accurate and very stable.

Finally, let us investigate the impacts of different weights. Fix the dataset size to be 1000, we vary the weight from 10^{-3} to 10^6 . As is shown in Fig.15, for the clean and Gaussian cases, both LAD-PINN and OLS-PINN with $\omega = 1.0$ reconstruct the physical field and recover the parameters relatively well. For all cases, LAD-PINN with $\omega = 1.0$ could achieve acceptable small errors. Therefore, choosing $\omega = 1.0$ might be appropriate in this subsection.

α	loss	Gaussian	Contaminated	Cauchy	Outlier	Mixed
0.05	LAD	2.446	2.322	2.073	3.187	3.304
	OLS	2.644	0.123	7.411	94.105	94.711
0.10	LAD	2.303	1.848	1.804	3.613	3.481
	OLS	2.814	7.379	35.793	98.799	98.314
0.15	LAD	2.609	2.274	1.199	2.676	2.682
	OLS	2.672	8.371	40.515	93.946	94.022
0.20	LAD	2.730	2.257	0.593	2.999	3.632
	OLS	2.932	15.652	38.493	94.681	93.448

Table 9: Relative errors(%) of the solution u to the wave equation with different corruption levels for $\#\mathbf{D}_u = 1000$.

α	loss	Gaussian	Contaminated	Cauchy	Outlier	Mixed
0.05	LAD	1.239	1.641	2.010	1.052	1.368
	OLS	0.899	3.472	117.890	200.846	205.928
0.10	LAD	2.086	2.438	3.090	1.766	2.595
	OLS	1.513	11.431	251.246	314.845	303.172
0.15	LAD	2.965	3.874	3.464	0.500	4.569
	OLS	2.169	11.030	385.941	367.705	362.870
0.20	LAD	3.673	5.121	4.748	0.667	8.476
	OLS	2.905	16.749	470.102	474.444	386.001

Table 10: Relative errors(%) of the recovered parameter c in the wave equation with different corruption levels for $\#\mathbf{D}_u = 1000$.

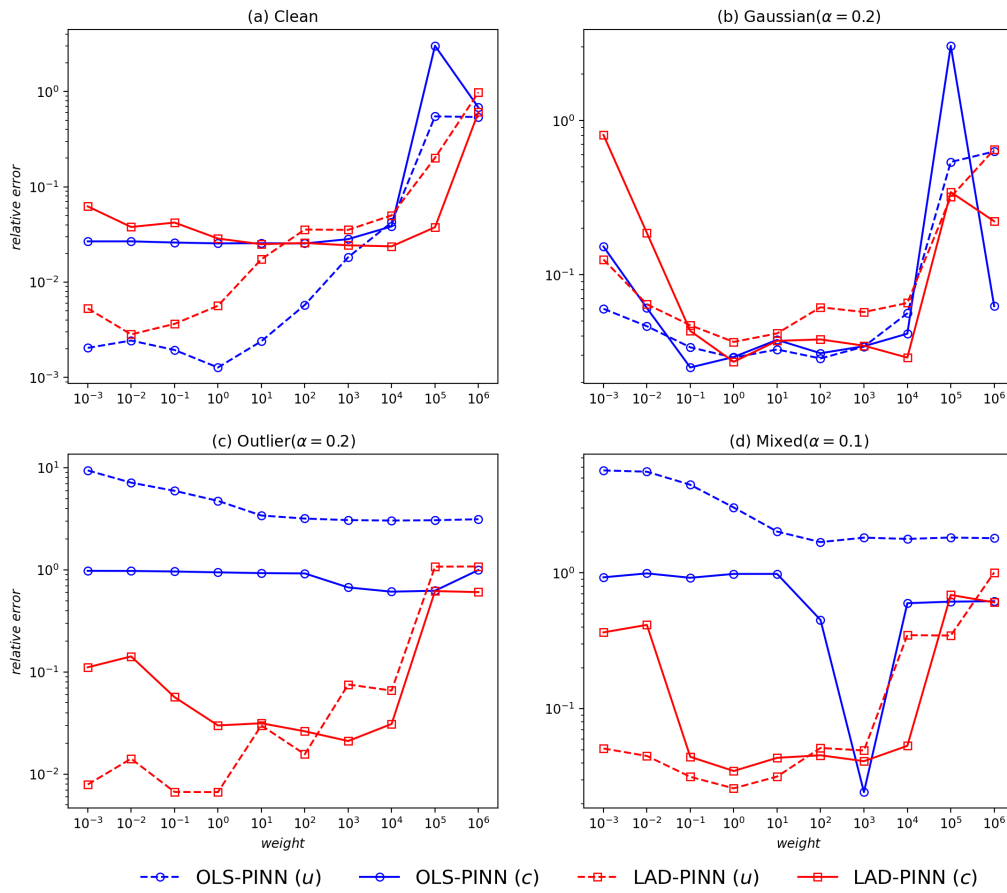


Figure 15: Effects of the weight parameter ω under different corruption types for the wave equation. ($\#\mathbf{D}_u = 1000$, $\alpha = 0.2$)

4.4. Unsteady 2D N-S equations with unknown parameters

In the last experiment, unsteady N-S equations are considered, the problem setup of which is referred to [1]. The N-S equations are explicitly given by

$$u_t + \lambda_1 (uu_x + vu_y) = -p_x + \lambda_2 (u_{xx} + u_{yy}) \quad (22)$$

$$v_t + \lambda_1 (uv_x + vv_y) = -p_y + \lambda_2 (v_{xx} + v_{yy}) \quad (23)$$

where λ_1 and λ_2 are two unknown parameters to be recovered. We make the assumption that

$$u = \psi_y, \quad v = -\psi_x$$

for some stream function $\psi(x, y)$. Under this assumption, the continuity equation will be automatically satisfied. The following architecture is used in this example,

$$\psi, p = \text{net}(t, x, y, \lambda_1, \lambda_2). \quad (24)$$

Note that unlike the neural network architecture used in Eq.(19), network (24) has only two equation constraints, while the former has six equation constraints. The advantage of network (19) is that it only requires solving the first-order derivatives while network (24) requires solving the third-order derivatives. Fewer loss terms or lower order derivatives may both make the training of PINN easier. The two architectures are not compared in this paper, which are only employed to illustrate the generalization of the proposed method.

Consider the rectangular region of interest (ROI) as shown in Fig.16.

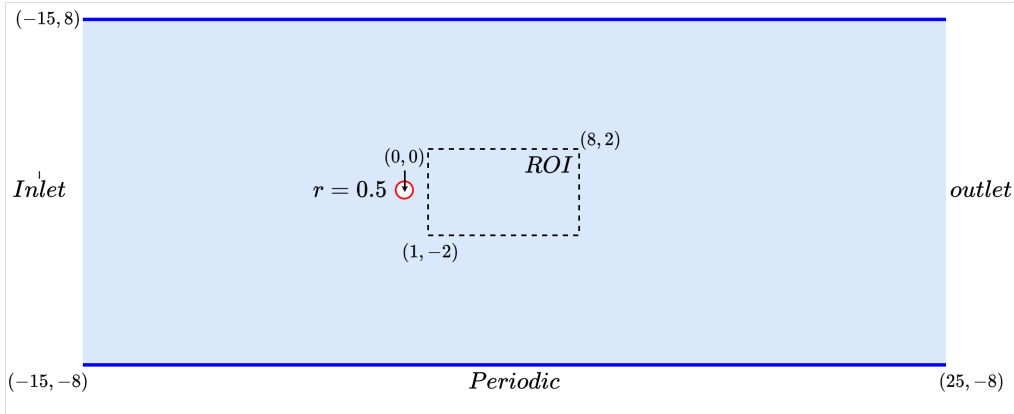


Figure 16: Problem setup of the unsteady N-S equation experiment. The spatio-temporal training data are sampled from the rectangular ROI behind the cylinder which is marked red. Refer to [1] for a detailed profile.

We set $\lambda_1 = 1.0$ and $\lambda_2 = 0.01$. An observation has the form of quintuple $(t_i, x_i, y_i, u_i, v_i)$, where pressure is hidden from observing. The data corruption setting is similar to Subsection 4.2.

For the recovery of λ_1 (Tab.11), we first consider fix $\#\mathbf{D}_u = 5000$. OLS-PINN performs much more accurate than LAD-PINN in four Gaussian cases and Contaminated cases under two lower corruption levels. When the data becomes more highly corrupted, LAD-PINN stays stable

α	loss	Gaussian	Contaminated	Cauchy	Outlier	Mixed
0.01	LAD	0.536	0.634	0.901	0.694	0.435
	OLS	0.162	0.276	2.459	100.109	99.961
0.05	LAD	0.651	0.588	0.804	1.392	1.009
	OLS	0.050	0.058	99.749	104.030	106.178
0.10	LAD	0.664	0.174	0.917	0.672	1.426
	OLS	0.014	0.702	99.943	99.621	99.548
0.20	LAD	0.857	1.038	1.301	1.690	4.062
	OLS	0.045	6.847	98.114	101.828	101.638

Table 11: Relative errors(%) of the recovered parameter λ_1 in the unsteady N-S equation with different corruption levels for $\#\mathbf{D}_u = 5000$.

α	loss	Gaussian	Contaminated	Cauchy	Outlier	Mixed
0.01	LAD	7.475	5.252	7.314	1.404	5.252
	OLS	8.542	10.755	67.498	100.047	100.062
0.05	LAD	3.613	9.728	9.294	12.161	2.975
	OLS	6.871	9.172	100.065	99.976	99.865
0.10	LAD	1.557	5.987	9.090	3.438	0.894
	OLS	3.740	17.366	100.166	99.961	99.997
0.20	LAD	10.564	12.006	9.069	5.681	12.439
	OLS	0.989	80.157	18.411	99.936	100.007

Table 12: Relative errors(%) of the recovered parameter λ_2 in the unsteady N-S equation with different corruption levels for $\#\mathbf{D}_u = 5000$.

while OLS-PINN begins to crash. In Tab.13, we fix $\alpha = 0.05$, which is small. Then OLS-PINN performs better than LAD-PINN in all Gaussian and Contaminated cases but worse than LAD-PINN in other highly corrupted cases.

For the recovery of λ_2 (Tab.12 and Tab.14). OLS-PINN performs similarly to its performance in the recovery of λ_1 . OLS-PINN recovers the parameter in less corrupted cases (Gaussian and Contaminated), but crashes in the remaining highly corrupted cases. Instead, LAD-PINN is much stable for the recovery of λ in all cases.

4.4.1. Reveal pressure via the two stage algorithms

Since the dynamic pressure field is hidden, we employ the two-stage framework to reveal the field from corrupted velocity observations. For a given moment t_p , the reconstructed pressure and the reference will differ by a constant. We define the constant by minimizing the squared norms:

$$\hat{c} = \arg \min_c \|p_{ref} - \hat{p} + c\|_2^2 \quad (25)$$

Due to the first-order optimality condition, we have

$$\hat{c} := \frac{\int_{\Omega} (\hat{p} - p_{ref}) dx dy}{\int_{\Omega} dx dy}. \quad (26)$$

N	loss	Gaussian	Contaminated	Cauchy	Outlier	Mixed
2000	LAD	0.377	1.263	1.123	0.831	1.009
	OLS	0.048	0.390	100.431	95.808	92.520
4000	LAD	0.844	0.921	1.050	1.094	0.760
	OLS	0.003	0.160	99.264	105.737	101.559
6000	LAD	0.578	0.813	0.897	0.801	0.609
	OLS	0.105	0.342	88.314	99.692	99.869
8000	LAD	0.500	0.495	0.452	0.651	0.592
	OLS	0.152	0.265	66.310	101.267	101.817

Table 13: Relative errors(%) of the recovered parameter λ_1 in the unsteady N-S equation with different dataset sizes for $\alpha = 0.05$.

N	loss	Gaussian	Contaminated	Cauchy	Outlier	Mixed
2000	LAD	1.488	0.656	6.401	1.557	0.514
	OLS	4.464	5.262	98.688	100.210	100.125
4000	LAD	3.068	7.197	0.827	2.848	3.895
	OLS	7.422	7.094	99.636	100.063	99.995
6000	LAD	3.784	5.889	6.806	2.006	3.549
	OLS	7.547	4.098	99.480	100.028	100.000
8000	LAD	4.451	5.455	0.326	1.479	0.969
	OLS	8.108	5.003	105.482	99.929	100.047

Table 14: Relative errors(%) of the recovered parameter λ_2 in the unsteady N-S equation with different dataset sizes for $\alpha = 0.05$.

Method		Clean	Gaussian	Contaminated	Cauchy	Outlier	Mixed
LAD	RE(%)	6.259	7.018	9.463	9.479	10.328	8.126
	# $\hat{\mathbf{D}}_u$	5000	5000	5000	5000	5000	5000
OLS	RE(%)	3.336	3.287	10.294	108.423	76.746	103.908
	# $\hat{\mathbf{D}}_u$	5000	5000	5000	5000	5000	5000
FR(0.1)	RE(%)	2.484	4.053	8.933	7.576	1.773	3.359
	# $\hat{\mathbf{D}}_u$	4500	4500	4500	4500	4500	4500
FR(0.2)	RE(%)	3.181	4.618	4.248	6.419	2.073	4.136
	# $\hat{\mathbf{D}}_u$	4000	4000	4000	4000	4000	4000
FR(0.3)	RE(%)	3.131	4.717	4.823	5.528	2.423	4.496
	# $\hat{\mathbf{D}}_u$	3500	3500	3500	3500	3500	3500
MAD(2.0)	RE(%)	2.885	3.814	4.592	6.618	2.259	3.589
	# $\hat{\mathbf{D}}_u$	4401	4936	4069	4015	4035	4453
MAD(2.5)	RE(%)	2.317	3.751	4.977	9.473	2.132	3.492
	# $\hat{\mathbf{D}}_u$	4597	4971	4123	4200	4176	4474
MAD(3.0)	RE(%)	2.116	3.542	4.822	8.416	2.164	3.669
	# $\hat{\mathbf{D}}_u$	4709	4981	4190	4336	4268	4477

Table 15: Relative errors(%) of the reconstructed pressure p in the unsteady N-S equation at $t = 10.0$ for $\#\hat{\mathbf{D}}_u = 5000$ and $\alpha = 0.1$: Bold numbers highlight the case with the best error for each corruption type.

Then we define the relative l_2 error to measure the accuracy of the reconstructed pressure as follows:

$$rel_p := \frac{\|p_{ref} - \hat{p} + \hat{c}\|_2}{\|p_{ref}\|_2}. \quad (27)$$

An snapshot at $t = 10.0$ is considered and the results are shown in Table 15. Except for the clean and Gaussian cases, the single-stage algorithm OLS-PINN cannot achieve an acceptable results, where the accuracy is very low or even explodes in all other cases. Single-stage LAD-PINN is usually less accurate, although it can reconstruct the pressure field under all kinds of data corruption. Two-stage algorithms can achieve more accurate results. Fig.17 shows the visualization results of the pressure at $t = 5.0, 10.0, 15.0$, and it can be seen that MAD-PINN has the smallest error among the three. This example demonstrates the ability of the two-stage methods to reveal hidden physics accurately.

5. Discussion and Conclusion

In order to apply PINN to a wide range of practical tasks, it is necessary to consider the cases involving anomalous data. Instead of employing data cleaning as a pre-processing step based on extra priors, this paper is mainly considered on the modeling level, proposing the LAD-PINN to deal with PDE reconstruction or coefficient identification problems involving high noise or anomalous data, as well as proposing a two-stage framework improve the accuracy further.

At the algorithm level, two issues remain to be addressed. One is the problem of loss weight selection when it is transformed into an unconstrained problem. However, no systematic methods exist to fix weights for varying noise scales. Fortunately, in the examples of this paper, weights

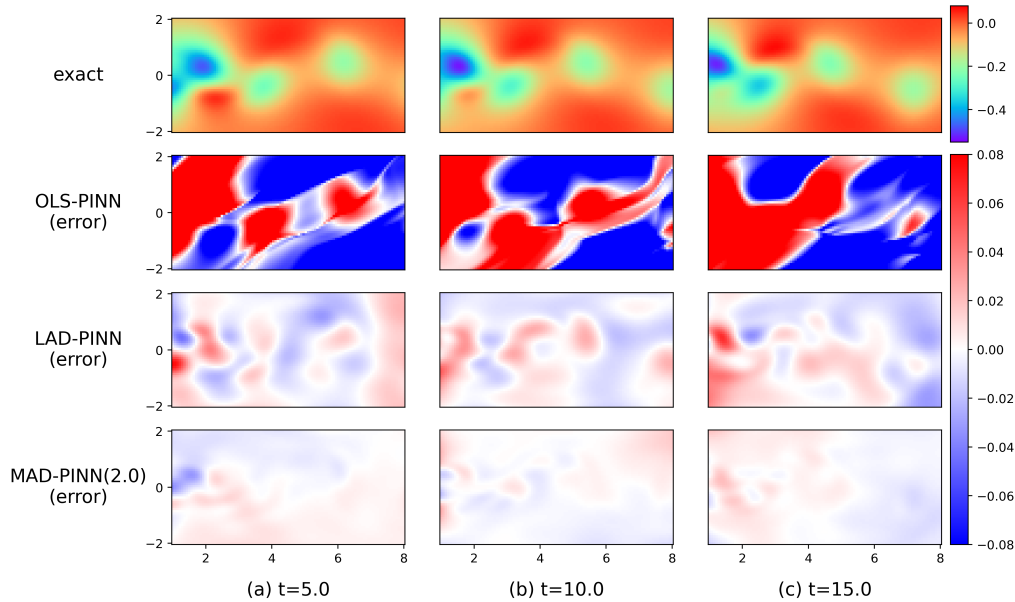


Figure 17: The snapshots of the ground truth pressure (the first row) and reconstruction errors (the last three rows) for the unsteady N-S equation. The magnitudes of OLS-PINN's error fall out of the colorbar.

of the losses have extensive acceptable ranges. The choice of weights may be avoided by using penalty methods or augmented Lagrangian multiplier methods, although both methods introduce more algorithmic hyperparameters while eliminating model hyperparameters. On the other hand, we did not specifically consider the non-smoothness of the LAD loss term in the computational sense. The loss term might be handled using reweighting methods like in robust analysis[45], which transform a non-smooth problem into sequential smooth subproblems. Of course, this approach also introduces more hyper-parameters, which are avoided as much as possible in this paper.

Acknowledgement

This work was supported by National Natural Science Foundation of China under Grant No.52005505 and 11725211.

References

- [1] M. Raissi, P. Perdikaris, G. E. Karniadakis, Physics-informed neural networks: A deep learning framework for solving forward and inverse problems involving nonlinear partial differential equations, *Journal of Computational Physics* 378 (2019) 686 – 707. doi:<https://doi.org/10.1016/j.jcp.2018.10.045>. URL <http://www.sciencedirect.com/science/article/pii/S0021999118307125>
- [2] M. Raissi, A. Yazdani, G. E. Karniadakis, Hidden fluid mechanics: Learning velocity and pressure fields from flow visualizations, *Science* 367 (6481) (2020) 1026–1030. doi:10.1126/science.aaw4741. URL <https://www.sciencemag.org/lookup/doi/10.1126/science.aaw4741>
- [3] S. Cai, Z. Mao, Z. Wang, M. Yin, G. E. Karniadakis, Physics-informed neural networks (PINNs) for fluid mechanics: a review, *Acta Mechanica Sinica* 37 (12) (2021) 1727–1738. doi:10.1007/s10409-021-01148-1. URL <https://doi.org/10.1007/s10409-021-01148-1>

- [4] X. Jin, S. Cai, H. Li, G. E. Karniadakis, NSFnets (Navier-Stokes flow nets): Physics-informed neural networks for the incompressible Navier-Stokes equations, *Journal of Computational Physics* 426 (2021) 109951. doi: 10.1016/j.jcp.2020.109951.
URL <https://linkinghub.elsevier.com/retrieve/pii/S0021999120307257>
- [5] L. Sun, H. Gao, S. Pan, J.-X. Wang, Surrogate modeling for fluid flows based on physics-constrained deep learning without simulation data, *Computer Methods in Applied Mechanics and Engineering* 361 (2020) 112732. doi: 10.1016/j.cma.2019.112732.
URL <https://linkinghub.elsevier.com/retrieve/pii/S004578251930622X>
- [6] E. Haghghat, M. Raissi, A. Moure, H. Gomez, R. Juanes, A physics-informed deep learning framework for inversion and surrogate modeling in solid mechanics, *Computer Methods in Applied Mechanics and Engineering* 379 (2021) 113741. doi:10.1016/j.cma.2021.113741.
URL <https://linkinghub.elsevier.com/retrieve/pii/S0045782521000773>
- [7] S. Cai, Z. Wang, S. Wang, P. Perdikaris, G. E. Karniadakis, Physics-Informed Neural Networks for Heat Transfer Problems, *Journal of Heat Transfer* 143 (6) (2021) 060801. doi:10.1115/1.4050542.
URL <https://asmedigitalcollection.asme.org/heattransfer/article/143/6/060801/1104439/Physics-Informed-Neural-Networks-for-Heat-Transfer>
- [8] Z. He, F. Ni, W. Wang, J. Zhang, A physics-informed deep learning method for solving direct and inverse heat conduction problems of materials, *Materials Today Communications* 28 (2021) 102719. doi:10.1016/j.mtcomm.2021.102719.
URL <https://linkinghub.elsevier.com/retrieve/pii/S235249282100711X>
- [9] L. Lu, R. Pestourie, W. Yao, Z. Wang, F. Verdugo, S. G. Johnson, Physics-Informed Neural Networks with Hard Constraints for Inverse Design, *SIAM Journal on Scientific Computing* 43 (6) (2021) B1105–B1132. doi:10.1137/21M1397908.
URL <https://epubs.siam.org/doi/abs/10.1137/21M1397908>
- [10] S. Wang, Y. Teng, P. Perdikaris, Understanding and Mitigating Gradient Flow Pathologies in Physics-Informed Neural Networks, *SIAM Journal on Scientific Computing* 43 (5) (2021) A3055–A3081. doi:10.1137/20M1318043.
URL <https://epubs.siam.org/doi/10.1137/20M1318043>
- [11] L. McClenny, U. Braga-Neto, Self-Adaptive Physics-Informed Neural Networks using a Soft Attention Mechanism, arXiv:2009.04544 [cs, stat] (Sep. 2020).
URL <http://arxiv.org/abs/2009.04544>
- [12] Z. Xiang, W. Peng, X. Liu, W. Yao, Self-adaptive loss balanced Physics-informed neural networks, *Neurocomputing* (2022) S092523122200546Xdoi:10.1016/j.neucom.2022.05.015.
URL <https://linkinghub.elsevier.com/retrieve/pii/S092523122200546X>
- [13] D. Liu, Y. Wang, A Dual-Dimer method for training physics-constrained neural networks with minimax architecture, *Neural Networks* 136 (2021) 112–125. doi:10.1016/j.neunet.2020.12.028.
URL <https://linkinghub.elsevier.com/retrieve/pii/S0893608020304536>
- [14] A. A. Ramabathiran, P. Ramachandran, SPINN: Sparse, Physics-based, and partially Interpretable Neural Networks for PDEs, *Journal of Computational Physics* 445 (2021) 110600. doi:10.1016/j.jcp.2021.110600.
URL <https://linkinghub.elsevier.com/retrieve/pii/S0021999121004952>
- [15] S. Wang, S. Sankaran, P. Perdikaris, Respecting causality is all you need for training physics-informed neural networks, *ArXiv* (2022). doi:10.48550/ARXIV.2203.07404.
URL <https://arxiv.org/abs/2203.07404>
- [16] J. Yu, L. Lu, X. Meng, G. E. Karniadakis, Gradient-enhanced physics-informed neural networks for forward and inverse PDE problems, *Computer Methods in Applied Mechanics and Engineering* 393 (2022) 114823. doi: 10.1016/j.cma.2022.114823.
URL <https://linkinghub.elsevier.com/retrieve/pii/S0045782522001438>
- [17] G. Raynaud, S. Houde, F. P. Gosselin, ModalPINN: An extension of physics-informed Neural Networks with enforced truncated Fourier decomposition for periodic flow reconstruction using a limited number of imperfect sensors, *Journal of Computational Physics* 464 (2022) 111271. doi:10.1016/j.jcp.2022.111271.
URL <https://linkinghub.elsevier.com/retrieve/pii/S0021999122003333>
- [18] X. Meng, Z. Li, D. Zhang, G. E. Karniadakis, PPINN: Parareal physics-informed neural network for time-dependent PDEs, *Computer Methods in Applied Mechanics and Engineering* 370 (2020) 113250. doi:10.1016/j.cma.2020.113250.
URL <https://linkinghub.elsevier.com/retrieve/pii/S0045782520304357>
- [19] A. D. J. . G. E. Karniadakis, Extended Physics-Informed Neural Networks (XPINNs): A Generalized Space-Time Domain Decomposition Based Deep Learning Framework for Nonlinear Partial Differential Equations, *Communications in Computational Physics* 28 (5) (2020) 2002–2041. doi:10.4208/cicp.0A-2020-0164.
URL http://global-sci.org/intro/article_detail/cicp/18403.html

- [20] S. Das, S. Tesfamariam, State-of-the-Art Review of Design of Experiments for Physics-Informed Deep Learning, arXiv:2202.06416 [cs, stat] (Feb. 2022).
URL <http://arxiv.org/abs/2202.06416>
- [21] M. A. Nabian, R. J. Gladstone, H. Meidani, Efficient training of physics-informed neural networks via importance sampling, *Computer-Aided Civil and Infrastructure Engineering* 36 (8) (2021) 962–977. doi:10.1111/mice.12685.
URL <https://onlinelibrary.wiley.com/doi/10.1111/mice.12685>
- [22] L. Lu, X. Meng, Z. Mao, G. E. Karniadakis, DeepXDE: A Deep Learning Library for Solving Differential Equations, *SIAM Review* 63 (1) (2021) 208–228. doi:10.1137/19M1274067.
URL <https://epubs.siam.org/doi/10.1137/19M1274067>
- [23] C. L. W. . J. Zhao, Solving Allen-Cahn and Cahn-Hilliard Equations using the Adaptive Physics Informed Neural Networks, *Communications in Computational Physics* 29 (3) (2021) 930–954. doi:10.4208/cicp.OA-2020-0086.
URL http://global-sci.org/intro/article_detail/cicp/18571.html
- [24] W. Peng, W. Zhou, X. Zhang, W. Yao, Z. Liu, RANG: A Residual-based Adaptive Node Generation Method for Physics-Informed Neural Networks (2022). doi:10.48550/ARXIV.2205.01051.
URL <https://arxiv.org/abs/2205.01051>
- [25] M. A. Fischler, R. C. Bolles, Random sample consensus: a paradigm for model fitting with applications to image analysis and automated cartography, *Communications of the ACM* 24 (6) (1981) 381–395. doi:10.1145/358669.358692.
URL <https://doi.org/10.1145/358669.358692>
- [26] C. Wang, S. Li, D. He, L. Wang, Is L2 physics-informed loss always suitable for training physics-informed neural network?, ArXiv abs/2206.02016 (2022).
- [27] G. Tran, R. Ward, Exact Recovery of Chaotic Systems from Highly Corrupted Data, *Multiscale Modeling & Simulation* 15 (3) (2017) 1108–1129. doi:10.1137/16M1086637.
URL <https://epubs.siam.org/doi/10.1137/16M1086637>
- [28] W. Peng, J. Zhang, W. Zhou, X. Zhao, W. Yao, X. Chen, IDRLnet: A Physics-Informed Neural Network Library, arXiv:2107.04320 [cs, math] (Jul. 2021).
URL <http://arxiv.org/abs/2107.04320>
- [29] D. P. Kingma, J. L. Ba, Adam: A method for stochastic optimization, in: 3rd International Conference on Learning Representations, ICLR 2015 - Conference Track Proceedings, 2015.
- [30] R. H. Byrd, P. Lu, J. Nocedal, C. Zhu, A Limited Memory Algorithm for Bound Constrained Optimization, *SIAM Journal on Scientific Computing* 16 (5) (1995) 1190–1208. doi:10.1137/0916069.
URL <https://epubs.siam.org/doi/abs/10.1137/0916069>
- [31] J. W. Demmel, *Applied Numerical Linear Algebra*, Society for Industrial and Applied Mathematics, 1997. doi:10.1137/1.9781611971446.
URL <http://epubs.siam.org/doi/book/10.1137/1.9781611971446>
- [32] P. Rousseeuw, V. Yohai, Robust Regression by Means of S-Estimators, in: J. Franke, W. Härdle, D. Martin (Eds.), *Robust and Nonlinear Time Series Analysis*, Lecture Notes in Statistics, Springer US, New York, NY, 1984, pp. 256–272. doi:10.1007/978-1-4615-7821-5_15.
- [33] P. J. Huber, Robust Estimation of a Location Parameter, *The Annals of Mathematical Statistics* 35 (1) (1964) 73–101. doi:10.1214/aoms/1177703732.
URL <http://projecteuclid.org/euclid.aoms/1177703732>
- [34] D. de Menezes, D. Prata, A. Secchi, J. Pinto, A review on robust M-estimators for regression analysis, *Computers & Chemical Engineering* 147 (2021) 107254. doi:10.1016/j.compchemeng.2021.107254.
URL <https://linkinghub.elsevier.com/retrieve/pii/S0098135421000326>
- [35] J. Steinhardt, P. W. Koh, P. Liang, Certified Defenses for Data Poisoning Attacks, in: *Proceedings of the 31st International Conference on Neural Information Processing Systems, NIPS'17*, Curran Associates Inc., Red Hook, NY, USA, 2017, pp. 3520–3532.
- [36] M. Yuan, Y. Lin, Model selection and estimation in regression with grouped variables, *Journal of the Royal Statistical Society: Series B (Statistical Methodology)* 68 (1) (2006) 49–67. doi:10.1111/j.1467-9868.2005.00532.x.
URL <https://onlinelibrary.wiley.com/doi/10.1111/j.1467-9868.2005.00532.x>
- [37] G. E. P. Box, Non-Normality and Tests on Variances, *Biometrika* 40 (3/4) (1953) 318. doi:10.2307/2333350.
URL <https://www.jstor.org/stable/2333350?origin=crossref>
- [38] S. Basir, I. Senocak, Physics and Equality Constrained Artificial Neural Networks: Application to Forward and Inverse Problems with Multi-fidelity Data Fusion, arXiv:2109.14860 [physics] (Feb. 2022).
URL <http://arxiv.org/abs/2109.14860>
- [39] D. Gervini, V. J. Yohai, A class of robust and fully efficient regression estimators, *The Annals of Statistics* 30 (2)

- (Apr. 2002). doi:10.1214/aos/1021379866.
 URL <https://projecteuclid.org/journals/annals-of-statistics/volume-30/issue-2/A-class-of-robust-and-fully-efficient-regression-estimators/10.1214/aos/1021379866.full>
- [40] C. Jennison, F. R. Hampel, E. M. Ronchetti, P. J. Rousseeuw, W. A. Stahel, Robust Statistics: The Approach Based on Influence Functions., *Journal of the Royal Statistical Society. Series A (General)* 150 (3) (1987) 281. doi:10.2307/2981480.
 URL <https://www.jstor.org/stable/2981480?origin=crossref>
- [41] C. Leys, C. Ley, O. Klein, P. Bernard, L. Licata, Detecting outliers: Do not use standard deviation around the mean, use absolute deviation around the median, *Journal of Experimental Social Psychology* 49 (4) (2013) 764–766. doi:10.1016/j.jesp.2013.03.013.
 URL <https://linkinghub.elsevier.com/retrieve/pii/S0022103113000668>
- [42] Y. Li, C. Wei, T. Ma, Towards explaining the regularization effect of initial large learning rate in training neural networks, in: *Proceedings of the 33rd international conference on neural information processing systems*, Curran Associates Inc., Red Hook, NY, USA, 2019.
- [43] C. Yu, W. Yao, Robust linear regression: A review and comparison, *Communications in Statistics - Simulation and Computation* 46 (8) (2017) 6261–6282. doi:10.1080/03610918.2016.1202271.
 URL <https://www.tandfonline.com/doi/full/10.1080/03610918.2016.1202271>
- [44] C. Rao, H. Sun, Y. Liu, Physics-informed deep learning for incompressible laminar flows, *Theoretical and Applied Mechanics Letters* 10 (3) (2020) 207–212. doi:10.1016/j.taml.2020.01.039.
 URL <https://linkinghub.elsevier.com/retrieve/pii/S2095034920300350>
- [45] G. Pitselis, A review on robust estimators applied to regression credibility, *Journal of Computational and Applied Mathematics* 239 (2013) 231–249. doi:10.1016/j.cam.2012.09.009.
 URL <https://linkinghub.elsevier.com/retrieve/pii/S0377042712003731>